An adaptive cruise control for connected energy-saving electric vehicles

Available online at www.sciencedirect.com

ScienceDirect

IFAC Papers Online CONFERENCE PAPER ARCHIVE

IFAC PapersOnLine 50-1 (2017) 2359–2364

An adaptive cruise control for connected energy-saving electric vehicles

Lorenzo Bertoni ** **Jacopo Guanetti** * **Maria Basso** **
Marco Masoero ** **Sabri Cetinkunt** *** **Francesco Borrelli** *

* *Department of Mechanical Engineering, University of California, Berkeley, CA. E-mail* {jacopoguanetti,fborrelli}@berkeley.edu
** *Dipartimento di Ingegneria Energetica, Politecnico di Torino, Italy. E-mail* marco.masoero@polito.it
*** *Department of Mechanical Engineering, University of Illinois at Chicago, Chicago, IL. E-mail* {scetin}@uic.edu

Abstract- We present an energy-saving cooperative adaptive cruise control (eco-CACC), which minimizes the energy consumption of autonomous electric vehicles. The approach leverages a trajectory preview from the preceding vehicle, and conciliates inter-vehicular distance reduction and speed profile smoothing. The problem is tackled with a nonlinear MPC approach. Rather than tracking a reference trajectory, our approach allows variations of distance and speed between vehicles, as long as the powertrain energy consumption is minimized and collision avoidance is guaranteed. Simulations show that this formulation can successfully handle real-world driving conditions, with limited computational complexity.

1. INTRODUCTION

A large portion of greenhouse gas emissions is caused by the transportation sector. Several approaches have been taken to counteract this situation, including the reduction of vehicles' energy consumption, and powertrain electrification. Even in electric vehicles, reducing energy consumption is important, because the electric grid power is not entirely produced from renewable sources, and because current on-board energy storage systems limit the driving range.

In recent years, research has shown that connectivity and driving automation can help reducing the energy consumption of vehicles. One approach is the so-called *eco-driving* (see e.g. Chang and Morlok (2005); Sciarretta et al. (2015)), which attempts to attain the energy-optimal speed trajectory, given constraints on the average speed and from the surrounding vehicles and infrastructure. Eco-driving may consider different levels of driving automation, but usually considers other vehicles as obstacles, if at all. On another front, the literature on driving automation started decades ago with studies on highway *platoons* (i.e. formations driving at the same speed and small inter-vehicular distance). While the main focus is on safety, stability, and road throughput maximization (see e.g. Lu et al. (2002); Swaroop and Hedrick (1999)), it is also clear that reducing the distance gaps between vehicles decreases the aerodynamic resistance, and hence the energy consumption (see e.g. Shladover et al. (2007); Solyom and Coelingh (2013)). However, exploitation of platooning to reduce energy consumption has been mostly been studied for heavy-duty vehicles, see e.g. Turri et al. (2016). A reason is that, in freight transportation, travel plans are defined in advance, there is some flexibility on the departure and arrival times, and therefore routing and platooning can be planned by a coordination center.

In this paper, we focus on electric vehicles for personal transportation. Our goal is to minimize energy consumption by suitably designing a Cooperative Adaptive Cruise Control (CACC) that leverages the existing literature and exploits connectivity and driving automation. Unless the platoon is driving at constant speed on a flat road, tracking the preceding vehicle's trajectory may result in a suboptimal speed profile, which may even nullify the energy savings due to reduced air drag (Al Alam et al. (2011)).

The focus of this paper is an energy-saving CACC (eco-CACC) that exploits a short-term trajectory preview from the preceding vehicle, and conciliates speed smoothing (to reduce powertrain losses) with the control of inter-vehicular distance (to reduce aerodynamic drag). The distance and velocity of two consecutive vehicles are kept bounded to ensure safety and maintain contact between platoon members; otherwise, distance and velocity can evolve freely, as the objective is to minimize the energy consumption.

A nonlinear model predictive control (MPC) approach is adopted. Our formulation does not explicitly pursue the regulation to an equilibrium point or the tracking of a reference trajectory, and it directly minimizes the vehicle's energy consumption. This approach is often referred to as *economic* MPC, see e.g. Ellis et al. (2014). The preview from the preceding vehicle is enabled by vehicle-to-vehicle (V2V) communication and by automated driving systems, which plan trajectories in advance and reliably follow them. In the absence of vehicle-to-vehicle communication, a prediction of the preceding vehicle's future trajectory can still be obtained, leveraging on-board measurements for automated driving.

The paper is organized as follows. The vehicle model is described in Section 2. Section 3 formulates the eco-CACC problem as an MPC problem. In Section 4, the

2405-8963 © 2017, IFAC (International Federation of Automatic Control) Hosting by Elsevier Ltd. All rights reserved.
Peer review under responsibility of International Federation of Automatic Control.
10.1016/j.ifacol.2017.08.425

eco-CACC performance is evaluated in simulation. Real-time implementation on an embedded platform is briefly investigated in Section 5. The paper ends with some concluding remarks.

2. VEHICLE MODEL

In this section, we present the vehicle model that is the basis of the proposed eco-CACC. The model encompasses the longitudinal dynamics and the powertrain of the electric vehicle (hereafter referred to as *ego vehicle*) implementing the eco-CACC. The preceding vehicle in the platoon formation is denoted as the *target vehicle*.

2.1 Longitudinal dynamics

As shown e.g. in Guzzella and Sciarretta (2013), longitudinal dynamics can quite accurately capture the mechanical energy consumption of a vehicle. In discrete time, Newton's second law and backward Euler approximation yield

$$\begin{aligned} v(t+1) &= v(t) + \frac{t_s}{m}\left(F_t(t) - F_b(t) - F_a(v(t), d(t)) - F_r\right), \\ s(t+1) &= s(t) + t_s v(t), \\ d(t) &= s_{\text{ref}}(t) - s(t), \end{aligned} \tag{1}$$

where m is the constant vehicle mass, F_t is the powertrain force, F_b is the friction braking force, F_a is the aerodynamic drag force and F_r is the rolling friction force. v and s denote the speed and position of the vehicle, respectively, while s_{ref} denotes the position of the target vehicle and d the distance between target and ego. The powertrain force is calculated as

$$F_t(t) = \frac{g_r}{r_w} T_m(t), \tag{2}$$

where T_m is the motor torque, r_w is the wheel radius and g_r is the gear ratio. Since we are considering an electric vehicle, we assume a fixed transmission ratio (see again Guzzella and Sciarretta (2013)). The aerodynamic resistance is defined as

$$F_a(v(t), d(t)) = \frac{1}{2}\rho A_f c_d(d(t)) v(t)^2, \tag{3}$$

where ρ is the air density, A_f is the frontal area of the vehicle, c_d is the air drag coefficient. The latter is a function of the distance between target and ego vehicle. It is well known that vehicles traveling at a short inter-vehicular distance enjoy reduced air resistance, due to the slipstream effect. In this work, we model c_d as a linear function of d, fitting experimental data from Hucho (1987). Fig. 1 shows a comparison between data and model.

The rolling resistance is expressed as

$$F_r = c_r m g, \tag{4}$$

where c_r is the (constant) rolling friction coefficient, and g is the gravitational constant. The effect of elevation is neglected here and will be the focus of future research.

2.2 Powertrain model

The powertrain model relates the longitudinal dynamics of the electric vehicles to the corresponding consumption of battery energy. Following again Guzzella and Sciarretta (2013), we use a quasi static approach to model the

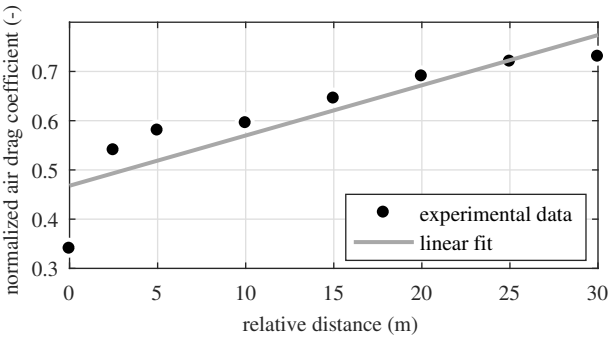

Figure 1. Dependence of the air drag coefficient c_d on the inter-vehicular distance d: experimental data from Hucho (1987) and linear fit.

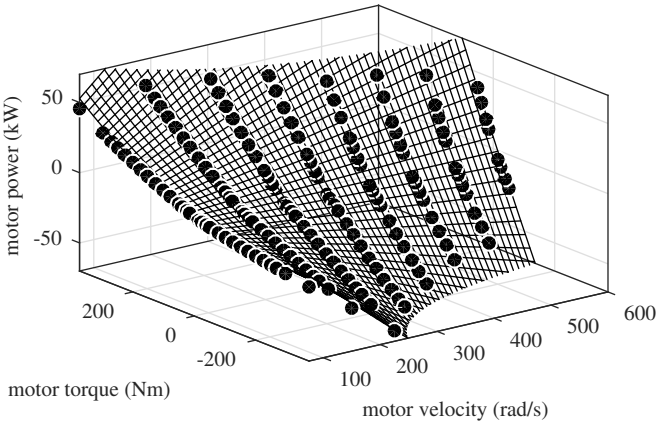

Figure 2. Powertrain data from QSS-TB (black dots) fitted with model (6).

powertrain. The electrical power absorbed (or generated) by the electric motor is given by

$$P_m(t) = T_m(t)\ \omega_m(t)\ \eta_m(T_m, \omega_m)^{-\text{sign}(T_m(t))}, \tag{5}$$

where T_m is the motor torque, ω_m is the rotational speed of the motor and η_m is the combined efficiency of transmission and motor. η_m is a function of both T_m and ω_m and is normally mapped through experiments. The latter is a function of vehicle speed, $\omega_m = \frac{g_r}{r_w} v$.

While generally accurate, model (5) is cumbersome for control design, and simplified models are often useful (see e.g. Sciarretta et al. (2015)). In this work, we adopt the model

$$P_m(t) = b_1 T_m(t)\omega(t) + b_2 T_m^2(t), \tag{6}$$

where b_1, b_2 are obtained with the following procedure. The efficiency map of a 12 kW electric motor was obtained from Guzzella and Amsutz (2005) and scaled to obtain a 60 kW motor. A transmission efficiency of 0.9 was included in the map (multiplying by 0.9 where $T_m \geq 0$ and dividing where $T_m < 0$). The resulting map was fitted with model (6), as shown in Fig. 2.

As a final note, any flow of power into or out of the battery (such as charging from the grid, supplying power to the traction motor, performing regenerative braking) is associated with losses due to the electrochemical conversion. Several modeling approaches exist for these losses, including equivalent circuits of the battery (see e.g. Guzzella

Table 1. Ego vehicle parameters.

m	vehicle mass	kg	1200
A_f	vehicle reference area	m^2	2
ρ	air density	kg/m^3	1.18
c_r	roll coefficient	-	0.008
r_w	wheel radius	m	0.3
b_1	powertrain model parameter	-	1.05
b_2	powertrain model parameter	-	0.18
t_s	sampling time	s	0.1

and Sciarretta (2013)). However, in eco-driving studies it is common (see e.g. Sciarretta et al. (2015) and the references quoted therein) to consider a constant battery efficiency or neglect it. In this work we follow this approach and optimize the electric energy output by the battery. The ego vehicle parameters are summarized in Table 1.

3. MPC FORMULATION

In this section, we formulate the eco-CACC problem and we propose an MPC approach to solve it in real-time.

3.1 Eco-CACC problem statement

The requirements for the controller are to exploit the preview from the target vehicle to (i) minimize the energy consumption of the ego vehicle, as defined in (6), and (ii) guarantee a minimum safe distance. Clearly, reducing the inter-vehicular distance reduces the air drag resistance and, therefore, the energy consumption under the same speed profile. However, aiming for the minimum distance may be counterproductive, particularly when the preceding vehicle has a variable speed profile: the power losses due to an aggressive tracking of the target vehicle may nullify the gains due the short inter-vehicular distance.

The system dynamics are defined in (1). The control inputs T_m and F_b are bounded

$$\begin{aligned} T_{\min} \leq T_m(t) &\leq T_{\max}\,, \\ F_{\min} \leq F_b(t) &\leq 0\,, \end{aligned} \tag{7}$$

where the torque bounds are assumed constant and symmetric, $T_{\min} = -T_{\max}$. The position of the ego vehicle is constrained by the position of the target vehicle, s_{ref}. This constraint is expressed in terms of the relative distance d

$$d_{\min} \leq d(t) \leq d_{\max}\,, \tag{8}$$

where $d_{\min}$ and $d_{\max}$ are the minimum and maximum distances between the ego and target vehicle. $d_{\min}$ is dictated by safety reasons (see Alam et al. (2014)), while, if $d_{\max}$ is exceeded, the platoon formation is considered broken. Finally, the speed of the ego vehicle is also constrained by

$$\begin{aligned} -\delta \leq v_{\text{ref}}(t) - v(t) &\leq \delta\,, \\ v_{\min}(t) \leq v(t) &\leq v_{\max}(t)\,, \end{aligned} \tag{9}$$

where v_{ref} denotes the speed of the target vehicle, δ is a bound on the relative speed, $v_{\min}$ and $v_{\max}$ are the minimum and maximum speed limits.

3.2 Eco-CACC MPC formulation

We now propose an MPC approach to solve in real time the eco-CACC problem stated above. At each time step t, the proposed controller solves the constrained finite time optimal control problem with horizon N

$$\min_{u(\cdot|t)} \quad J = p(x(t+N|t) + \sum_{k=t}^{t+N-1} g(x(k|t), u(k|t)) \tag{10a}$$

$$\text{s.t.} \quad x(k+1|t) = f(x(k|t),\, u(k|t),\, v_{\text{ref}}(k|t))\,, \tag{10b}$$

$$d(k|t) = s_{\text{ref}}(k|t) - s(k|t), \tag{10c}$$

$$d_{\min} \leq d(k|t) \leq d_{\max}\,, \tag{10d}$$

$$v_{\min}(t) \leq v(k|t) \leq v_{\max}(t)\,, \tag{10e}$$

$$-\delta \leq v_{\text{ref}}(k|t) - v(k|t) \leq \delta \tag{10f}$$

$$\forall k = t, ..., t+N,$$

$$T_{\min} \leq T_m(k|t) \leq T_{\max}\,, \tag{10g}$$

$$F_{\min} \leq F_b(k|t) \leq 0\,, \tag{10h}$$

$$\forall k = t, ..., t+N-1,$$

$$x(t|t) = x(t)\,, \tag{10i}$$

where $x = [s\ v]^T$, $u = [T_m\ F_b]^T$, f denotes the dynamics in (1), and the running cost is $g = P_m$ as defined in (6). The previews of the target vehicle trajectory, s_{ref} and v_{ref}, are assumed known throughout the MPC prediction horizon. A terminal cost p is also introduced, as detailed below.

3.3 Terminal cost design

In an application like CACC, an MPC formulation without terminal penalty or constraints risks to be myopic in many situations. We then introduce a terminal penalty to make the MPC longsighted, without extending the prediction horizon and consequently worsen the computational burden to solve problem (10). The proposed terminal penalty encompasses two terms, one for the terminal velocity and one for the terminal position

$$p(x(t+N|t)) = p_v(x(t+N|t)) + p_s(x(t+N|t))\,. \tag{11}$$

Penalization of the terminal velocity Pure minimization of the running cost along the prediction horizon disregards the fact that kinetic energy is conservative. A trajectory with high terminal speed may have high running cost, but also high terminal kinetic energy. The optimal trajectory depends on the velocity of the target vehicle, not only along the MPC prediction horizon, but also afterwards. In the absence of further information, it is reasonable to assume that the target vehicle will maintain a constant velocity after the end of the prediction horizon

$$v_{\text{ref}}(t+N+j|t) = v_{\text{ref}}(t+N),\ \forall j \geq 0. \tag{12}$$

In such a scenario, the ego vehicle would also end up at the same speed $v_{\text{ref}}(t+N)$, possibly after a transient. A logical choice is then to penalize the difference of kinetic energy at the end of the prediction horizon between target and ego vehicle

$$p_v(v(t+N|t)) = \frac{1}{2} b_k m \left(v_{\text{ref}}(t+N|t)^2 - v(t+N|t)^2\right), \tag{13}$$

where b_k is a tuning coefficient to account for powertrain losses linked with speed oscillations.

Penalization of the terminal distance The air drag reduction encourages the ego vehicle to follow the target at a small distance; however, the pure minimization of the running cost along the prediction horizon may lead to another locally optimal solution, in which the ego vehicle

Table 2. MPC controller parameters

N	MPC horizon	-	100
$d_{\min}$	minimum distance	m	2
$d_{\max}$	maximum distance	m	20
$T_{\min}$	minimum motor torque	N m	−100
$T_{\max}$	maximum motor torque	N m	100
$F_{\min}$	minimum braking force	kN	30
δ	relative speed bound	m/s	3
b_k	powertrain losses coefficient	-	1.028

reduces its speed to travel the minimum possible distance. In closed loop, this would bring the ego vehicle to follow the target at $d = d_{\max}$. This is also a problem of myopia, as the distance not traveled along the horizon will have to be traveled anyway later.

To counteract this effect, we focus on the energy lost in friction (i.e. due to forces F_a and F_r in (1)) along the MPC horizon. This energy loss, which we denote by ΔE_f, is a function of the terminal position of the ego vehicle, which is constrained by that of the target vehicle,

$$s(t+N|t) \leq s_{\text{ref}}(t+N|t) - d_{\min}\,. \tag{14}$$

Thus, also the energy lost in friction is bounded by $\Delta E_f(s_{\max}(t+N|t))$, where $s_{\max}(t+N|t)$ denotes the upper bound on the ego vehicle position. We penalize the deviation from this upper bound

$$\Delta E_f(s_{\max}(t+N|t)) - \Delta E_f(s(t+N|t))\,. \tag{15}$$

Friction is a non conservative force, so we consider its average value along the MPC horizon

$$\Delta E_f(s) \approx \underbrace{\frac{\rho A_f \bar{c}_d}{2N^2 t_s^2}}_{A} s^3 + \underbrace{c_r g m}_{B} s \tag{16}$$

where s denotes the distance traveled by the ego vehicle along the horizon, and $\bar{c}_d$ represents the air drag coefficient at the initial distance $d(t)$.

Plugging (16) into (15) returns a cubic function of the terminal position $s(t+N|t)$. However, the result can also be written as a function of the terminal distance $d(t+N|t)$. After straightforward calculations we obtain (we omitted the time index $(t+N|t)$ for brevity)

$$A(d^3 - 3d^2 s_{\max} + 3d s_{\max}^2) + Bd\,, \tag{17}$$

where $-d^3 + 3d^2 s_{\max} \ll 3d s_{\max}^2$ for normal values of d and $s_{\max}$. Therefore, we neglect them and define the penalty on the terminal distance as

$$p_s(x(t+N|t)) = (3A s_{\max}(t+N|t)^2 + B)(s_{\max}(t+N|t) - s(t+N|t)). \tag{18}$$

The MPC parameters are summarized in Table 2.

4. SIMULATION ANALYSIS

In this section, we evaluate the performance of the proposed eco-CACC in different simulation scenarios, and compare its energy consumption with that of a baseline ACC approach.

4.1 Simulation setup

Solution of the nonlinear optimization problem Problem (10) must be solved every time step $t_s = 100\,\text{ms}$. In our simulations, this nonlinear optimization problem was solved with IPOPT (Wächter and Biegler (2006)), an efficient interior point solver for nonlinear optimization problems.

Baseline ACC strategy The energy performance of the eco-CACC was compared with a baseline ACC, that just requires the ego vehicle to follow the target vehicle at a fixed distance. It is implemented as a tracking MPC, using the longitudinal dynamic model (1) and setting as reference signals the preceding vehicle speed v_{ref} and the inter-vehicle spacing d. The latter should generally be a function of the vehicles' speed for safety reasons. In this work we keep it constant along the scenario, for simplicity.

Simulation of the target vehicle In our simulations, we assumed to receive a perfect forecast of the target vehicle trajectory, with the same length as the prediction horizon N of the MPC. The trajectories of the target vehicle were real vehicle trajectories, collected in both highway and urban driving using on-board sensors. The vehicle was equipped with a radar and an OTS RT2002 system, which includes a differential GPS (global positioning system), an IMU (inertial measurement unit) and a DSP (digital signal processor). In an experimental setting, these data may be used to tune and validate algorithms for the prediction of the target vehicle trajectory.

Vehicle energetics simulator The energy consumption under the two ACC approaches was estimated using the Quasi-Static Toolbox (QSS-TB), see Guzzella and Amsutz (2005). QSS-TB is a Simulink blockset which estimates fuel and energy consumption for a number of powertrains. It belongs to the family of so-called *backward facing* powertrain simulators, i.e. those that reconstruct the fuel/energy consumption given the speed profile of the vehicle (Guzzella and Sciarretta (2013)).

While QSS-TB still uses quasi-static models, it accounts for aspects that were neglected in the model presented in Section 2, namely transmission idle power, electric motor inertia and battery efficiency depending on current and state of charge. Additionally, we modified the air drag resistance, which in QSS-TB is not position dependent. For better agreement with the data from Hucho (1987), instead of the linear relation used in Section 2, we used the formula (see Turri et al. (2016))

$$c_d(d) = c_{d,0}\left(1 - \frac{c_{d,1}}{c_{d,2} + d}\right), \tag{19}$$

where $c_{d,0}$ is the nominal air drag coefficient (i.e. its value when there is no preceding vehicle, $d \to \infty$) and $c_{d,1}$ and $c_{d,2}$ are fitting parameters.

4.2 Highway scenario

In this scenario, both the ego and the target vehicle are traveling in the highway at an initial velocity of 20 m/s. The initial distance between the two vehicles is 12 m, and the target vehicle is accelerating. Fig. 3 shows the trajectories of the distance, speed and motor torque. In the first 10 seconds, the ego vehicle increases its speed and catches up with the target vehicle, to take advantage of the reduced air drag at a close inter-vehicular distance.

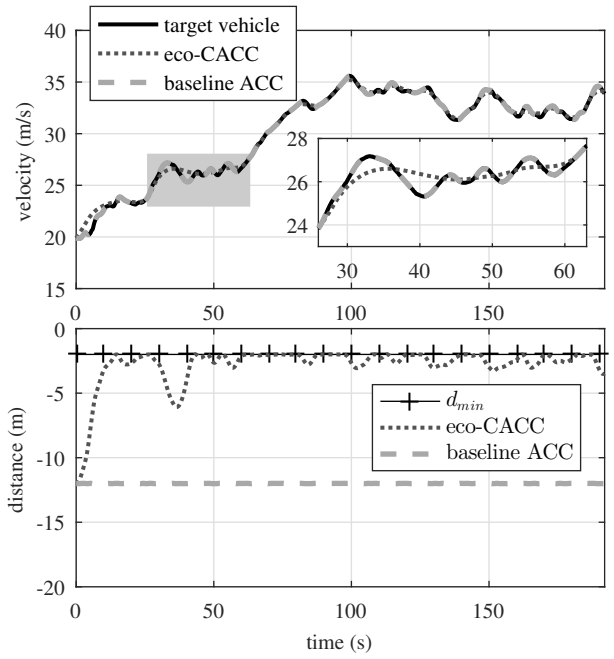

Figure 3. Velocity (top) and inter-vehicular distance (bottom) of the target and ego vehicle, using the eco-CACC and the baseline ACC in the highway scenario.

Afterwards, the distance is not kept constant, but it is continuously adapted to conciliate air drag reduction with the energy losses linked to an aggressive tracking of the target vehicle. As a result, the ego vehicle has a smoother speed profile.

The eco-CACC was also compared to a baseline ACC; the selected metrics were the energy consumption per unit distance, the RMS value of the relative distance d, and the RMS value of the jerk. With the baseline ACC, the ego vehicle follows the target vehicle at a fixed distance, equal to the initial distance; it does not catch up to reduce the distance, nor does it smooth the speed profile. Therefore, the comparison highlights how the performance of the eco-CACC benefits from managing both the inter-vehicular distance and the powertrain forces. In this scenario, the energy consumption with the eco-CACC is found to be 15.6 % lower than with the baseline ACC. This is achieved with a combination of distance reduction and speed smoothing; in particular, the jerk RMS is about 70 percent less. On the other hand, the eco-CACC consumes additional energy in the catch up phase (until second 10, approximately).

In general highway driving, the energy savings will depend on the behavior of the target vehicle, on the minimum distance $d_{\min}$ and on the target distance for the baseline ACC. The goal of this simulation study is to illustrate the

Table 3. Performance in the highway scenario using the eco-CACC and the baseline ACC.

ACC strategy	Energy (W h/km)	RMS(d) (m)	RMS($\dot{a}$) (m/s^3)
baseline ACC	149	12	0.234
eco-CACC	126	3.2	0.069

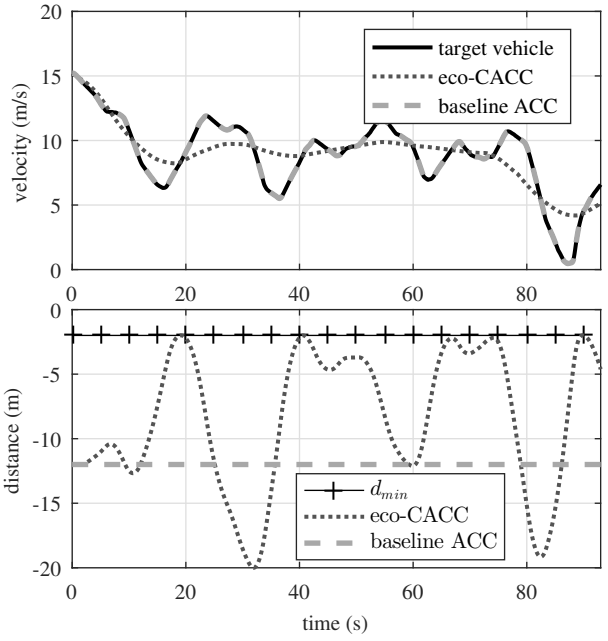

Figure 4. Velocity (top) and inter-vehicular distance (bottom) of the target and ego vehicle, using the eco-CACC and the baseline ACC in the urban scenario.

proposed eco-CACC concept. A comprehensive comparison will be the object of future research.

4.3 Urban Scenario

In this scenario, the target vehicle follows a trajectory that was recorded in urban driving. As it can be observed in Fig. 4, its speed has large variations, due to the surrounding traffic. Compared to the highway scenario, here the eco-CACC is much less aggressive in pursuing a small inter-vehicular distance. Although the target vehicle is initially decelerating (hence reducing the distance gap can be achieved by simply coasting), the ego vehicle initially maintains a distance between 10 and 12 m. Afterwards, it maintains an almost constant speed of about 10 m/s, while the relative distance oscillates between $d_{\min}$ and $d_{\max}$ due to the speed variations of the target vehicle.

Overall, in this scenario the eco-CACC judges more convenient to sacrifice the air drag reduction in favor of a smoother speed profile, which substantially reduces powertrain losses. Also notice that, compared to the highway scenario, the air drag resistance is reduced due to the lower speed. The predicted energy consumption with the eco-CACC is 73.4 % lower than with the baseline ACC. This is to be considered an upper bound to performance, for a number of reasons. In an urban context, the reliability of the target vehicle preview may significantly decrease, due to the surrounding traffic. The ego vehicle itself may incur in more restrictive speed and position constraints,

Table 4. Performance in the urban scenario using the eco-CACC and the baseline ACC.

ACC strategy	Energy (W h/km)	RMS(d) (m)	RMS($\dot{a}$) (m/s^3)
baseline ACC	64	12	0.315
eco-CACC	16	9.9	0.072

Table 5. Average and peak computational time t_c in the scenario of Section 5.

	average t_c (ms)	peak t_c (ms)
IPOPT (laptop)	81.5	118.1
FORCES Pro (laptop)	29.4	47.7
FORCES Pro (dSpace)	47.8	52.5

due to other vehicles cutting in and pedestrians crossing the road. Also, the baseline ACC is quite stiff and a less aggressive controller could achieve better performance in this scenario.

In an MPC framework, the above aspects can be considered including an uncertain model of the environment, see e.g. Carvalho et al. (2015). The corresponding problem can be tackled applying robust or stochastic MPC techniques. While these approaches introduce some conservatism, the significant energy savings found suggest optimism. The investigation of this direction requires richer datasets to characterize the uncertainty in the target vehicle preview, and is therefore left to future research.

5. EMBEDDED IMPLEMENTATION

The simulations presented in the previous section were performed in a non-real-time setting, using Matlab and Simulink on a laptop. In this section, we used FORCES Pro (Domahidi and Jerez (2014)) to automatically generate a tailored solver for problem (10). The solver is generated as self-contained C code, which enables the implementation on embedded platforms and the verification of real-time performance.

We evaluate the embedded implementation in a basic highway scenario. Both the ego and the target vehicle start at a speed of about 22 m/s and at a distance of 12 m. The target vehicle accelerates for about 10 s and afterwards maintains a constant speed of about 30 m/s. The ego vehicle accelerates in the initial phase, to catch up with the target vehicle; afterwards, it follows at the minimum distance $d_{\min}$.

The resulting MPC controller was implemented and executed in real time on a dSpace MicroAutobox 1401, which includes an IBM PowerPC processor capable of running at 800 MHz. Table 5 summarizes the average and peak values of the computational time t_c, for a sampling time $t_s = 0.1$ s and an MPC horizon $Nt_s = 8$ s. The comparison with IPOPT on the same platform (a laptop with Intel Core i7-4710HQ, 2.5 GHz) shows a reduction of about 64 % in the average t_c, and of about 60 % in the peak t_c. The implementation on dSpace MicroAutobox shows that t_c is well below the sampling time t_s, thus the real-time implementation of the proposed eco-CACC is possible.

6. CONCLUSIONS

In this paper, we presented an eco-CACC approach to minimize the energy consumption in autonomous electric vehicles. Using a nonlinear MPC formulation, we exploit a preview from the preceding vehicle and control that of the ego vehicle. Rather than tracking a reference trajectory, our approach seeks the optimal trade off between air drag reduction due to reduced inter-vehicular distance, and powertrain energy losses, due to suboptimal speed profile. Simulations in real-world driving conditions show significant improvements when compared to a baseline ACC approach. Implementation on an embedded platform demonstrates the feasibility of real-time implementation. Future work will address implementation on real vehicles and robustness to forecast uncertainty.

REFERENCES

Al Alam, A., Gattami, A., Johansson, K.H., and Tomlin, C.J. (2011). Establishing safety for heavy duty vehicle platooning: A game theoretical approach. In *18th IFAC World Congress*, volume 18, 3818–3823.

Alam, A., Gattami, A., Johansson, K.H., and Tomlin, C.J. (2014). Guaranteeing safety for heavy duty vehicle platooning: Safe set computations and experimental evaluations. *Control Engineering Practice*, 24, 33–41.

Carvalho, A., Lefévre, S., Schildbach, G., Kong, J., and Borrelli, F. (2015). Automated driving: The role of forecasts and uncertainty—A control perspective. *European Journal of Control*, 24, 14–32.

Chang, D.J. and Morlok, E.K. (2005). Vehicle speed profiles to minimize work and fuel consumption. *Journal of transportation engineering*, 131(3), 173–182.

Domahidi, A. and Jerez, J. (2014). FORCES Professional. embotech GmbH (url: http://embotech.com/FORCES-Pro).

Ellis, M., Durand, H., and Christofides, P.D. (2014). A tutorial review of economic model predictive control methods. *Journal of Process Control*, 24(8), 1156–1178.

Guzzella, L. and Amsutz, A. (2005). *The QSS Toolbox Manual*. Institute of Energy Technology ETH Zurich.

Guzzella, L. and Sciarretta, A. (2013). *Vehicle Propulsion Systems - Introduction to Modeling and Optimization*. Springer-Verlag Berlin Heidelberg, 3 edition.

Hucho, W.H. (1987). *Aerodynamics of road vehicles*. Butterworth-Heinemann.

Lu, X.y., Hedrick, J.K., and Drew, M. (2002). ACC/CACC - Control Design, Stability and Robust Performance. In *American Control Conference (ACC), 2002*, 4327–4332.

Sciarretta, A., Nunzio, G.D., and Ojeda, L.L. (2015). Optimal Ecodriving Control: Energy-Efficient Driving of Road Vehicles as an Optimal Control Problem. *IEEE Control Systems Magazine*, 35(5), 71–90.

Shladover, S.E. et al. (2007). Path at 20-history and major milestones. *IEEE Transactions on intelligent transportation systems*, 8(4), 584–592.

Solyom, S. and Coelingh, E. (2013). Performance limitations in vehicle platoon control. *IEEE Intelligent Transportation Systems Magazine*, 5(4), 112–120.

Swaroop, D. and Hedrick, J. (1999). Constant spacing strategies for platooning in automated highway systems. *Journal of dynamic systems, measurement, and control*, 121(3), 462–470.

Turri, V., Besselink, B., and Johansson, K.H. (2016). Cooperative look-ahead control for fuel-efficient and safe heavy-duty vehicle platooning. *IEEE Transaction on Control System Technology*, (Available online).

Wächter, A. and Biegler, L.T. (2006). On the implementation of an interior-point filter line-search algorithm for large-scale nonlinear programming. *Mathematical programming*, 106(1), 25–57.